Russ. J. Numer. Anal. Math. Modelling, Vol. 27, No. 4, pp. 399–412 (2012)
DOI 10.1515/ rnam-2012-0022

CFD technology for 3D simulation of large-scale hydrodynamic events and disasters

Yu. V. VASSILEVSKI*, K. D. NIKITIN*, M. A. OLSHANSKII†, and K. M. TEREKHOV*

Abstract — In this paper we discuss the basic components of the computational technology for the simulation of complex hydrodynamic events, such as a break of a dam, a wave pileup, a landslide, or a mud flow. The technology uses three-dimensional equations of fluid dynamics with free boundaries. The mathematical model is based on the Navier–Stokes equations with nonlinear defining relations between the stress tensor and the rate of strain tensor. The assignment of a particular defining relation allows one to simulate both Newtonian flows (break of a dam, wave pileup), and non-Newtonian ones (landslide, mud flow, snow avalanche, flood of lava). The numerical model developed in the paper uses the method of the grid level set function for calculation of a free surface flow evolution and adaptively reconstructed three-dimensional grids of the octree type for discretization of the flow equations. The predictive accuracy of this technology is demonstrated in the paper by comparing the results of certain numerical calculations with physical experiments; the efficiency of the technology is illustrated by simulation of the break of a dam and a mud flow using the actual 3D topology of the area around the Sayano-Shushenskaya dam.

Mathematical modelling is an efficient tool to predict scenarios and consequences of anthropogenic disasters and natural phenomena. Modelling large-scale hydrodynamic events, such as the break of a dam, tsunami wave pileup, landslide, or mud flow, snow avalanche, or lava eruption plays a significant role. The variety of phenomena and possible scenarios generates many approaches to their numerical simulation. As an example, we note the modelling of oceanic anomalies with the use of ocean dynamics equations [27], the spread of tsunami based on shallow water equations [24, 30], landslide and debris flow simulation based on different modifications of hydrodynamics equations [14], calculation of a flood of lava with the use of discrete dynamic systems [8] or snow avalanches runout using dynamic equations for granulated mixtures [22].

In this paper we study an approach allowing one to simulate various events and phenomena listed above taking into account their actual physical and geometric complexity. Standard simplifications based on the 'shallow water' theory or on

*Institute of Numerical Mathematics of the Russian Academy of Sciences, Moscow. Corresponding author. E-mail: yuri.vassilevski@gmail.com

†Mechanical and Mathematical Dept. of the Moscow M. V. Lomonosov State University, Moscow. E-mail: Maxim.Olshanskii@mtu-net.ru.

The work was partly supported by the Russian Foundation for Basic Research (11–01–00971, 11–01–00767, 12–01–00283) and by the Federal Target Program Scientific and Scientific-Pedagogical Personnel of Innovative Russia.

model dimension reduction are not used in this paper. Calculations are performed for a complete three-dimensional system of hydrodynamic equations for flows with free boundaries. The phenomenological variety of considered processes is reflected in a special choice of defining relations for the stress tensor. We consider both Newtonian media (water) and viscoplastic ones (landslide), but the technology developed here does not prevent a researcher or a user from choosing other probably more complex defining relations.

The numerical method developed in this paper is based on several important methods and technologies. We use the level set method [29] for defining the evolution and finding the position of a free boundary and also adaptively refined octree grids. Octree grids combine the simplicity of orthogonal grids, the possibility of hierarchical refining (in this paper we use refining toward the free boundary), the convenience of data access, and fast reconstruction. As a consequence, nowadays such grids have become widespread in numerical simulations and animation, see, e.g., [15, 18, 20, 21, 25]. The integration in time is performed by the splitting scheme of Temam–Chorin–Yanenko type. One step in time is split into convective transport, addition of diffusive and plasticity terms, projection on the space of discrete-divergence-free functions, and advective transfer of the level set function. The velocity is approximated on a staggered grid, i.e., the velocity components are assigned to the centers of faces, the pressure is positioned at the centers of cells. The spatial approximation of advective transport uses the semi-Lagrangian method, a finite-difference scheme is used for the diffusion and plasticity terms, the Poisson equation for the pressure is approximated by the finite volume method. It is known that this discretization satisfies the Ladyzhenskaya–Babuska–Brezzi condition and is stable on such grids. Numerical experiments suggest that stability of this type is retained on octree meshes. Note once again that it is the combination of the approaches mentioned above, i.e., the level set method, dynamic octree grids, splitting schemes, and compact and stable finite differences, that ensures realistic and predictive simulation of complex three-dimensional flows with a free boundary.

The remainder of the paper is organized as follows. In Section 1 we present the mathematical model. Section 2 describes the computational technology for numerical solution of the differential model. Further we verify the numerical approach by comparing the results of numerical and physical experiments for models of Newtonian and viscoplastic flows. These results are presented in Section 3. Finally, Section 4 shows the application of the numerical technology for simulation of such events as the break of the dam at the Sayano-Shushenskaya hydro power plant and a landslide in the vicinity of the dam. Both experiments were performed taking into account the real topography of the region and do not require computational resources exceeding the capacity of an ordinary (state-of-the-art) workstation.

1. Mathematical model

The mass and momentum conservation laws for an incompressible viscous non-Newtonian fluid in Euler's formulation lead to the Navier–Stokes equations for the

unknown fluid velocity $\mathbf{u}$ and stress tensor τ:

$$\begin{cases} \rho\left(\dfrac{\partial \mathbf{u}}{\partial t} + (\mathbf{u}\cdot\nabla)\mathbf{u}\right) - \mathbf{div}\,\tau = \mathbf{f} \\ \nabla\cdot\mathbf{u} = 0 \end{cases} \quad \text{in } \Omega(t) \tag{1.1}$$

where $\mathbf{f}$ are given mass forces, $\Omega(t) \in \mathbb{R}^3$ is a spatial domain occupied by the fluid and dependent on time, ρ is the density. The system is supplied with defining relations linking the stress tensor and the rate of strain tensor: $\mathbf{Du} = [\nabla\mathbf{u} + (\nabla\mathbf{u})^T]/2$. We use the following nonlinear Hershel–Bulkley relations [12] for viscoplastic media:

$$\begin{aligned} \tau = -p\mathbf{I} + \left(K\,|\mathbf{Du}|^{n-1} + \tau_s|\mathbf{Du}|^{-1}\right)\mathbf{Du} \;&\Leftrightarrow\; |\tau| > \tau_s \\ \mathbf{Du} = \mathbf{0} \;&\Leftrightarrow\; |\tau| \leqslant \tau_s \end{aligned} \tag{1.2}$$

where K is the consistency parameter, τ_s is the yield stress parameter, n is the fluid index, $|\mathbf{Du}| = \left(\sum_{1\leqslant i,j\leqslant 3}|D_{ij}\mathbf{u}|^2\right)^{1/2}$, $\mathbf{I}$ is the unit tensor ($\mathbf{I}_{ij} = \delta^i_j$), the scalar function p denotes the pressure. Particular values of the parameters ρ, K, τ_s, and n are tuned for the most accurate modelling of rheological properties of the considered medium. Thus, $\tau = 0$, $n = 1$ correspond to Newtonian flows (e.g., water without admixtures), relations with $\tau > 0$ and $n \neq 1$ can be applied to model non-Newtonian flows, such as snow avalanches, underwater landslides, debris flows, or flood of lava [2,4,5,16].

In order to overcome the well-known difficulties related to the indeterminateness of the stress tensor in relations (1.2) inside the plug and rigid zones, i.e., where the rate of strain tensor equals zero, we use the regularization of Bercovier–Engelman [3] which is reduced to the replacement of $|\mathbf{Du}|$ by $|\mathbf{Du}|_\varepsilon = \sqrt{|\mathbf{Du}|^2 + \varepsilon^2}$ with some small parameter ε. This allows us to write down the equations of fluid dynamics in the whole volume $\Omega(t)$ and exclude the stress tensor:

$$\begin{cases} \rho\left(\dfrac{\partial \mathbf{u}}{\partial t} + (\mathbf{u}\cdot\nabla)\mathbf{u}\right) - \mathbf{div}\,\mu_\varepsilon\mathbf{Du} + \nabla p = \mathbf{f} \\ \nabla\cdot\mathbf{u} = 0 \end{cases} \quad \text{in } \Omega(t). \tag{1.3}$$

The 'efficient' viscosity parameter is introduced into system (1.3):

$$\mu_\varepsilon = K\,|\mathbf{Du}|_\varepsilon^{n-1} + \tau_s|\mathbf{Du}|_\varepsilon^{-1}$$

and it depends nonlinearly on the rate of deformations.

We suppose that the volume occupied by the fluid and the initial flow are given at the initial time moment $t = 0$:

$$\Omega(0) = \Omega_0, \quad \mathbf{u}|_{t=0} = \mathbf{u}_0. \tag{1.4}$$

Finding $\Omega(t)$ for $t > 0$ is a part of the problem which is solved together with equations (1.3). To give its mathematical formulation, we divide the boundary of the

whole volume into the static boundary Γ_D (for example, the rigid walls or the bottom of the basin) and the free boundary $\Gamma(t)$ (typically this is the water-air interface, i.e., $\overline{\partial\Omega(t)} = \overline{\Gamma_D} \cup \overline{\Gamma(t)}$. In our calculations we neglect the influence of the surrounding gas (air) onto the liquid. Therefore, the mathematical model is presented for the liquid–vacuum idealization. However, if necessary, the influence of the surrounding gas can be taken into account in the model and calculated without any additional difficulties. Note also that, generally speaking, the static boundary Γ_D can depend on time.

We assume the non-penetration conditions on the static boundary and, depending on the considered flow, the nonslip or slip with friction conditions. The free boundary evolves with normal velocity components on the boundary, which is written in the form of the kinematic relation

$$v_\Gamma = \mathbf{u} \cdot \mathbf{n}_\Gamma \tag{1.5}$$

where $\mathbf{n}_\Gamma$ is the outer unit normal to the surface $\Gamma(t)$, v_Γ is the normal velocity of the surface $\Gamma(t)$. The balance conditions of the surface tension forces and the normal stresses of the medium also hold on the free surface, which leads to the boundary condition

$$\tau\mathbf{n}_\Gamma = \varsigma\varkappa\mathbf{n}_\Gamma - p_{\text{ext}}\mathbf{n}_\Gamma \quad \text{on } \Gamma(t) \tag{1.6}$$

where $\varkappa$ is the sum of the principal curvatures of the surface, ς is the surface tension coefficient, p_{ext} is the external pressure. If the surface tension forces are not taken into account, we may assume $\varsigma = 0$.

In order to find the position of the free boundary at each time moment, instead of (1.5) we use the implicit definition of $\Gamma(t)$ as the zero level set of the globally defined function $\varphi(t,\mathbf{x})$:

$$\varphi(t,\mathbf{x}) \begin{cases} < 0, & \mathbf{x} \in \Omega(t) \\ > 0, & \mathbf{x} \in \mathbb{R}^3 \setminus \overline{\Omega(t)} \\ = 0, & \mathbf{x} \in \Gamma(t) \end{cases} \qquad \forall t \in [0,T].$$

The function φ is called the *level set function* in the literature. Initial condition (1.4) allows us to determine the initial $\varphi(0,\mathbf{x})$. At any time moment $t > 0$, the level set function satisfies the following transport equation [23]:

$$\frac{\partial\varphi}{\partial t} + \widetilde{\mathbf{u}} \cdot \nabla\varphi = 0 \quad \text{in } \mathbb{R}^3 \times (0,T] \tag{1.7}$$

where $\widetilde{\mathbf{u}}$ is the fluid velocity field extended outside $\Omega(t)$. Note that one often poses the additional restriction

$$|\nabla\varphi| = 1 \tag{1.8}$$

onto the level set function to ensure numerical stability, i.e., φ is the signed distance function. Given φ, the outer normal and the curvature of the free boundary can be calculated by the formulas $\mathbf{n}_\Gamma = \nabla\varphi/|\nabla\varphi|$ and $\varkappa = \nabla \cdot \mathbf{n}_\Gamma$.

The mathematical model used in our calculations consists of equations (1.3), (1.4), (1.6)–(1.8) and appropriate boundary conditions on static boundaries.

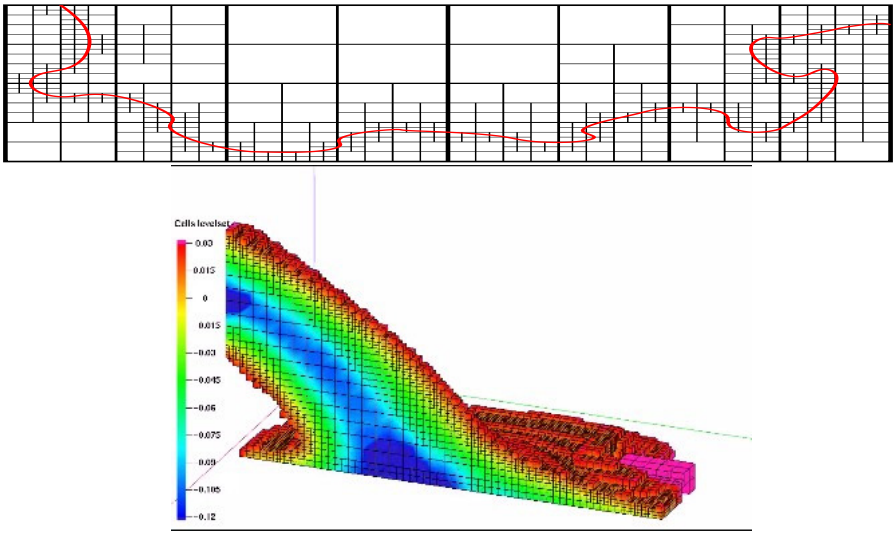

Figure 1. 2D quad-tree greed is refined towards the free boundary (top). 3D adaptively refined octree grid (cross-section) and values of the level set function at a fixed time moment in the test problem of flooding a container with an object inside (bottom).

2. Fundamentals of computing technology

The free boundary of a fluid may have a complicated geometry in actual hydrodynamic scenarios. As a consequence, an adequate representation of this geometry and simulation of surface dynamics require grids with a sufficiently fine spatial resolution in the neighbourhood of $\Gamma(t)$. The use of uniform grids for three-dimensional problems becomes too burdensome from the computational viewpoint in this case. Locally refined and/or coarsened grids require significantly less computational resources. However, if a free boundary evolves, then adaptive grids have to be reconstructed according to the surface evolution. Grid reconstruction can be sufficiently efficient from the viewpoint of computational cost if we use structured octree grids instead of tetrahedral ones traditionally used in finite element methods. A two-dimensional analogue of the grids used in our calculations is presented in Fig. 1 (top). An octree grid pattern in the experiment of filling a container with a water spurt is shown for a certain time moment in Fig. 1 (bottom). An efficient access and operations with data defined on the octree grids use their natural hierarchical structure; details can be found, e.g., in monograph [26].

The grid adaptation strategy used in this work is based on its gradual refinement in the neighbourhood of the free boundary at the current time moment t in the neighbourhood of $\Gamma(t+\Delta t)$, so that the sizes of two adjacent cells cannot differ more than twice. Here Δt is the step in time.

In order to discretize equations (1.3) with respect to spatial variables, we use a stable scheme on staggered grids. In this scheme the unknown velocity components are assigned to the faces of cells (the ith velocity component is approximated at the

center of the cubic cell which is orthogonal to the ith coordinate axis) and the pressure is approximated at the centers of cells. This location of the unknowns ensures the mass conservation law for the discrete solution locally for each cell of the partition. The level set function is approximated at the vertices of cells. Finite-difference analogues of differential operators on such grids are discussed in detail in [19].

The discretization in time utilizes the approach based on the Chorin–Temam–Yanenko splitting scheme [6]. Given $\mathbf{u}(t)$, $p(t)$, $\varphi(t)$ at a current time moment, one time step consists in the determination of $\mathbf{u}(t+\Delta t)$, $p(t+\Delta t)$, $\varphi(t+\Delta t)$ and is split into several substeps. First we update the level set function and calculate the new domain occupied by the fluid, $\Omega(t) \to \Omega(t+\Delta t)$. At this step, we use the method of numerical integration along the characteristics for the transport equation (1.7), which is also known as the semi-Lagrangian method [28]. In this case the equation for the characteristics is integrated with the second order of accuracy. Due to approximation errors, the numerical integration of equation (1.7) may lead and often does lead to an erroneous loss or gain of the fluid volume, i.e., $|\Omega(t)| \neq |\Omega(t+\Delta t)|$ without the outflow (or inflow) of the fluid. The loss of volume decreases with adaptation of the grid to the boundary and with the use of the method of particles [11]. An additional correction is performed by finding the constant δ from the equation

$$\operatorname{meas}\{\mathbf{x} : \varphi(\mathbf{x}) \leqslant \delta\} = \operatorname{Vol}^{\text{reference}}$$

and further correction $\varphi^{\text{new}} = \varphi - \delta$. The value of δ is calculated by the secant method, and the Monte-Carlo method is used for an approximate calculation of $\operatorname{meas}\{\mathbf{x} : \varphi(\mathbf{x}) < \delta\}$. Further we apply the reinitialization of φ^{new}, so that the resulting level set function is the signed distance function. The details of the reinitialization used here can be found in [19, 20]. At this step, the calculation of the new flow domain $\Omega(t) \to \Omega(t+\Delta t)$ is finished, the reconstruction of the grid is performed, and all variables are interpolated from the old grid to the new one. In the process of interpolation and integration of equation (1.7) we have to calculate an extension of the velocity function $\mathbf{u}(t)$ from $\Omega(t)$ into the whole computation domain. In this case the extension is built constant along the normals to the free boundary, i.e., $(\nabla\varphi)\cdot\nabla\mathbf{u}(t) = 0$ outside of $\Omega(t)$.

The second part of the time step of the splitting scheme consists in finding the new values of hydrodynamic variables in $\Omega(t+\Delta t)$: $\{\mathbf{u}(t), p(t)\} \to \{\mathbf{u}(t+\Delta t), p(t+\Delta t)\}$. The procedure is divided into several substeps according to the classic splitting scheme:

- the convective step is performed by the semi-Lagrangian method;
- the viscous and plasticity terms are added;
- the obtained velocity field is projected onto the space of divergence-free vector functions by solving the grid Poisson equation for the pressure.

The stability of the numerical integration of the system is ensured by the choice

of the time step satisfying the Courant condition

$$\Delta t = \min\left\{ C_1 h_{\min}\left(\max_{\mathbf{x}\in\Omega(t)} |\mathbf{u}(t)|\right)^{-1}, \quad C_2 \rho^{\frac{1}{2}} h_{\min}^{\frac{3}{2}} \varsigma^{-\frac{1}{2}} \right\}$$

where C_1 and C_2 are parameters dependent on a particular application. In most numerical calculations we have taken $C_1 = 0.66$ and $C_2 = 1.4$.

3. Verification of the method

In this section we present the results of few numerical experiments for model flows. The results are compared with experimental data and demonstrate a high predicting ability of the numerical method.

The first test is the problem of an instantaneous collapse of a water column in a horizontal channel of a rectangular cross-section (see, e.g., [10]). A schematic setup of the problem is shown in Fig. 2 (left). At the initial time moment the fluid is in its rest state and bounded by a unit cube, i.e., $x = y = h = 1$. At the next time moment, the fluid column collapses under the action of the force of gravity directed along the axis z. The values of the parameters K, ρ, ς (viscosity, density, surface tension coefficient) in the experiments were taken to simulate a water flow. In particular, $\tau_s = 0$ and $n = 1$. The statistics we are interested in is the position of the bottom ream front point of the water depending on time. The calculations were performed on a sequence of octree grids. Each grid was obtained by a refinement of the previous one. The results of numerical experiments are presented in Fig. 2 (right) where they are compared with experimentally measured values from [17] (the time shift of -0.007 s is used for the results, which corresponds to the time of the gate opening). It is well seen that, starting from the value corresponding to the minimal size of a cell equal to $1/256$, the calculation results do not visually differ from each other and match well the results of physical experiments.

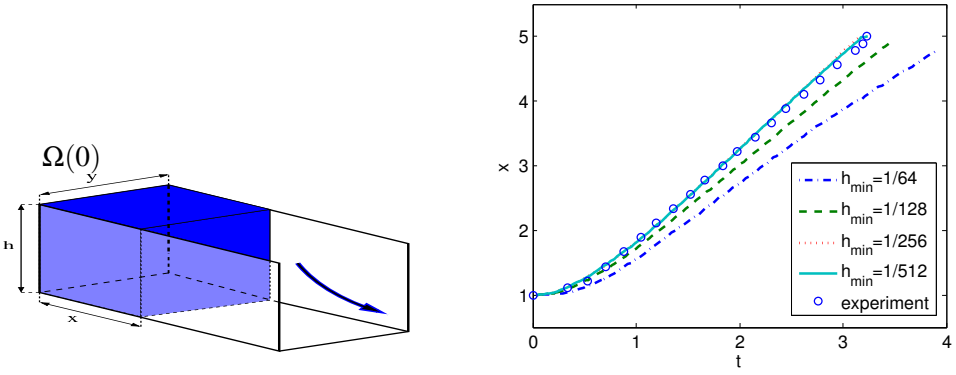

Figure 2. Left: the schematic setup of the problem of an instantaneous collapse of a water column in a horizontal channel. Right: Graphs of the x-coordinate of the center point of water bottom ream obtained in calculations with different minimal sizes of octree grid cells. Comparison is done with experimental data from [17].

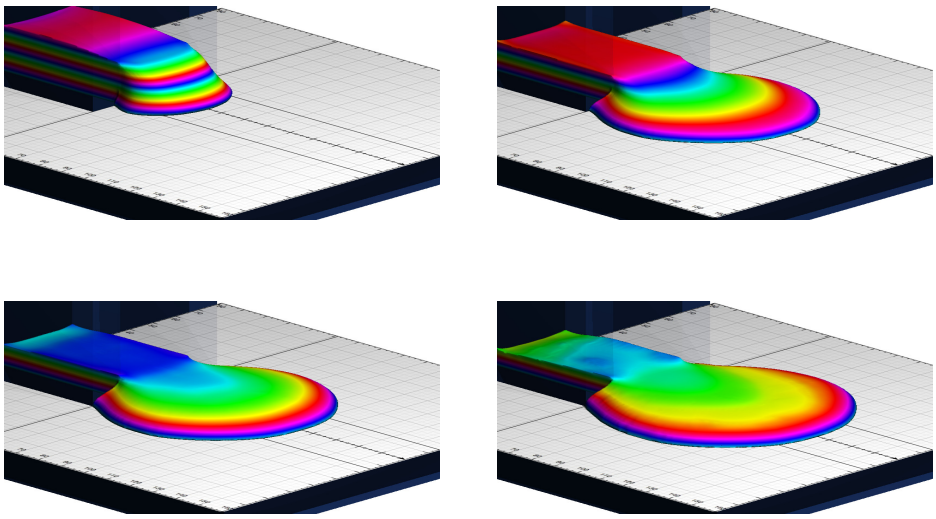

Figure 3. Outflow of a viscoplastic fluid from a tank over an inclined plane. Different colors correspond to different depths. The solution calculated numerically is shown for the inclination angle $\alpha = 12^o$ at the time moments $t \in \{0.2, 0.6, 1.0, 2.0\}$ s.

The next experiment is the numerical simulation of a viscoplastic flow over an inclined plane. The importance of viscoplastic flows over inclined planes in practical problems causes great interest in calculation and analysis of such flows (see, e.g., a detailed review in [1, 13]). In contrast to many other studies, the present technology allows one to calculate such flows with all their complexity taking into account the effects of inertia, surface tension, and a complex three-dimensional geometry.

The following experiment is simulated numerically: consider a plane inclined at an angle α to the horizon. A rectangular tank with the length X and width Y is placed onto the plane. The tank is filled with a viscoplastic medium of volume V. We assume that the rheology of the medium satisfies the Herschel–Bulkley law. The side of the tank positioned lower on the inclined plane has a gate perpendicular to the plane. When the gate is opened, the fluid is released and flows downwards the inclined plane. An example of the flow is shown for different time moments in Fig. 3.

The numerical experiments were performed with the set of parameters corresponding to the physical experiments from [7]: $X = 0.51$ m, $Y = 0.3$ m, $V = 0.06$ m^3, $\alpha \in \{12^\circ, 18^\circ\}$, and the following set of rheological parameters for the Herschel–Bulkley model: $K = 47.68$ Pa s^{-n}, $n = 0.415$, $\tau_s = 89$ Pa. It was found in [7] that the Herschel–Bulkley model with these parameters sufficiently well approximates the rheology of 0.3% Carbopol Ultrez 10 used in physical experiments. Further details of the numerical experiments and calculations with other values of the parameters can be found in [20].

Figure 4 shows the evolution of the middle profile of the fluid free surface for

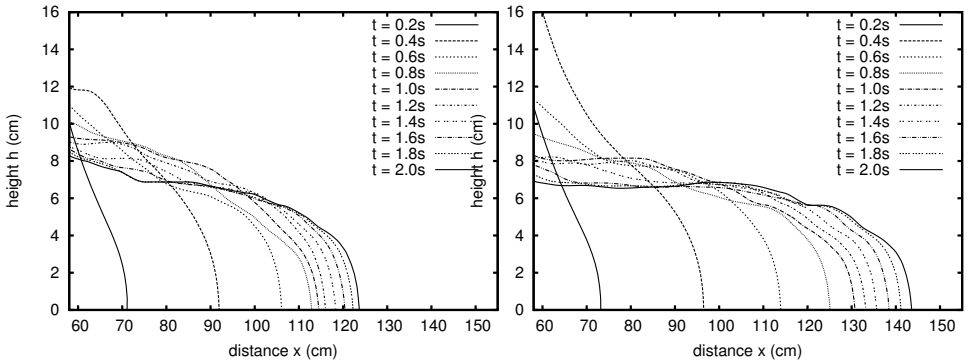

Figure 4. Middle profiles of the free flow surface at the time moments $t = 0.2k$ (s), $k = 1, \ldots, 10$ for different plane inclination angles: (a) $\alpha = 12^\circ$, (b) $\alpha = 18^\circ$.

different inclination angles of the plane (note the different scaling in the abscissa and ordinate axes), these graphs are in a good agreement with the data (similar graphs) of the real viscoplastic material from the experiments in [7]. It is clearly seen from these graphs that the fluid begins to flow sufficiently fast at the initial moment and then slows down sharply around the time moment of $t = 0.8$ s. After that the front of the fluid continues moving over the inclined plane slower and more or less uniformly. Note that such dual behaviour of the viscoplastic flow obtained by numerical calculations is in excellent correspondence with experimental observations. In particular, describing the fluid dynamics in experiments with a Carbopol solution, the authors of [7] pointed out: '... we observed two regimes: at the very beginning ($t < 1$ s), the flow was in an inertial regime; the front velocity was nearly constant. Then, quite abruptly, a pseudo-equilibrium regime occurred, for which the front velocity decayed as a power-law function of time'. Note that the time scale of this physical experiment was about 8 hours, whereas we stopped our calculations for $t = 2$ s and did not study the asymptotic behaviour of the flow.

Summing up, we point out that the mathematical model and the numerical technology developed here predict the qualitative behaviour and statistically meaningful characteristics of three-dimensional flows of Newtonian and viscoplastic fluids. We have illustrated this by comparing the results of numerical calculations and physical experiments. This allows us to use these model and technology for predictive simulation of large-scale hydrodynamic events (such as the break of a dam, snow avalanches, landslide etc. using the real region topology). Some examples of such calculations are presented in the next section.

4. Some calculations of large-scale hydrodynamic events

As an example of numerical simulation of large-scale hydrodynamics events (disasters), we present the calculation of the consequences of the break of the dam and

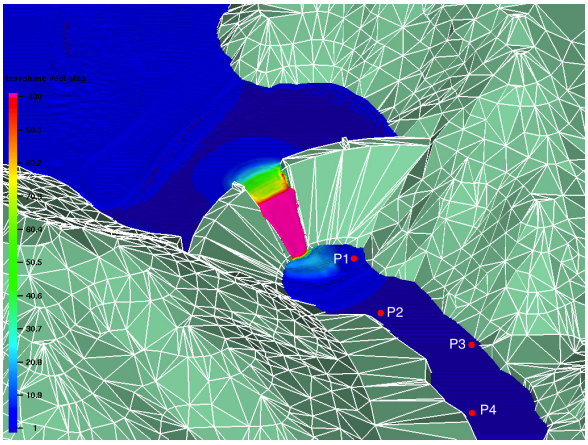

Figure 5. The dam and surrounding area. The points where the monitoring of the water level variation is performed are marked in the figure. Different colors indicate the magnitude of the fluid velocity vector.

the landslide at the Sayano-Shushenskaya dam. Note that the calculations presented below do not simulate actual or possible disaster scenarios for this hydro power, but only show that such simulations are *practically possible* with the use of the technology described here in the presence of more detailed geophysical data for the riverside area and the dam conditions. In these calculations we have used the topographic map of the area obtained with the help of the Shuttle Radar Topography Mission (NASA) [31], the resolution of this map is about 90 m. We used the Google SketchUp to construct a polygonal approximation of the dam and the earth surface in the neighbourhood of the dam. The computational domain and the part of the dam simulated as 'broken' are shown in Fig. 5.

We are interested in computing the following data: the water rise level at given points (points P1–P4 are indicated in Fig. 5) and the pressure onto the base of the dam at the tail-water under the spillway. The obtained results are shown as graphs in Fig. 6 (in this section all variables are dimensional and given in the SI system).

The following calculation simulates a rock landslide on the left-bank slope near the dam. Since more accurate data were absent, the landslide simulation was performed using the Herschel–Bulkley model of a viscoplastic medium with the coefficients K, τ_s, n taken from [4], where these coefficients were chosen so that the model describe well the rheological properties of rock landslides in the Puglia region in the south of Italy. We recall that simulation of realizable scenarios possibly requires additional data concerning the properties of the rocks and the conditions of the slopes in the region; in our case we have no such data.

In the simulation of the landslide we are interested in the final deposit of landslide and the pressure acting on the dam structures at the place of the landslide. Figure 7 shows the top view at the final and intermediate time moments of the cal-

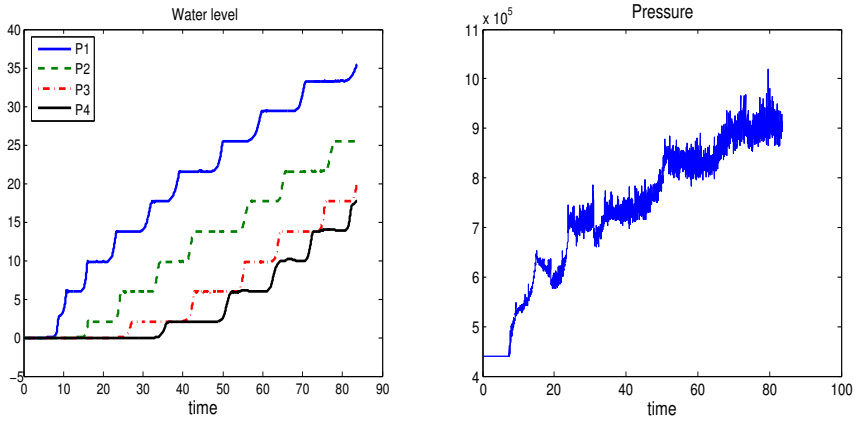

Figure 6. Dependence of water level on time at points P1–P4 (left). Graph of the pressure over the base of the dam at the tail-water under the spillway (right).

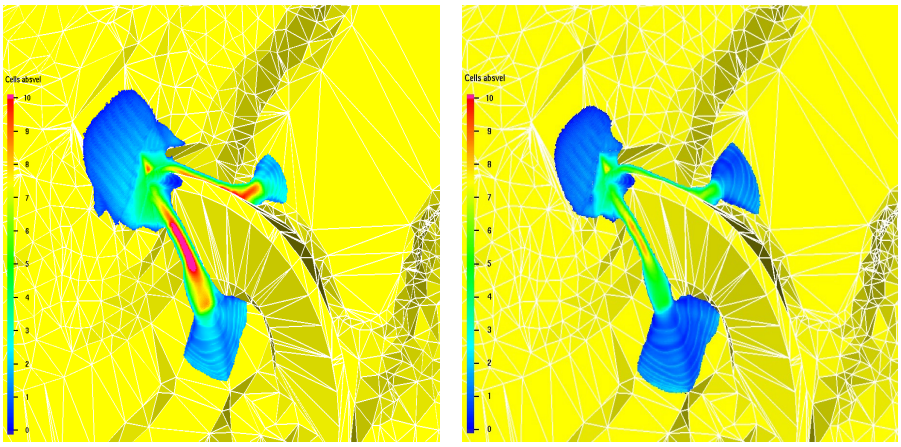

Figure 7. Migration of the landslide at time moments $t = 100$s and $t = 167$ s. Different colors mark the velocity vector magnitudes for the particles of the landslide.

culation. The variation of the total kinetic energy of the whole landslide masses in time is shown in Fig. 8 (right). Note that the landslide has lost a considerable part of its kinetic energy by the end of the calculations, thus, it is reasonable to assume that we have determined the final deposit of the landslide masses. The graph of the maximal pressure onto the body of the dam at the place of the landslide is given in Fig. 8 (left). Note that the maximal number of cubic cells slightly exceeded 520 and 560 thousand in the simulation of an emergency spill through a dam break and the landslide calculation, respectively.

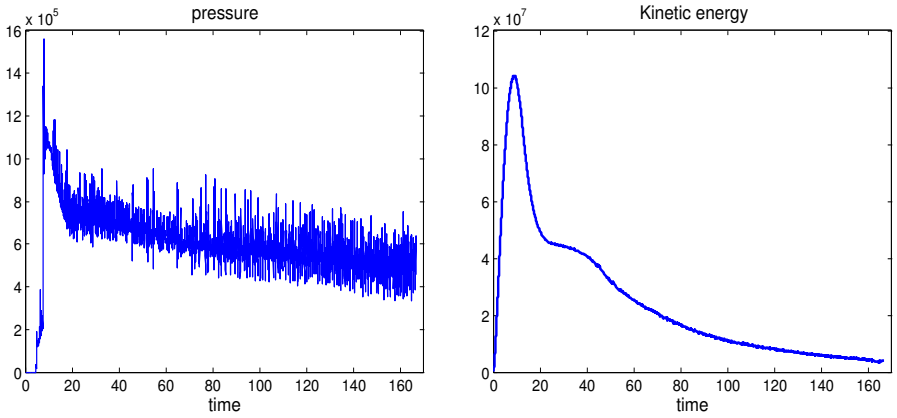

Figure 8. Pressure onto the dam body at the place of the landslide. Variation of the kinetic energy of the whole landslide mass in time.

Conclusion

In this paper we have presented a numerical technology allowing one to simulate complex hydrodynamic events based on three-dimensional equations of continuous medium with free boundaries. The accuracy and reliability of this numerical approach has been tested on model academic problems. The abilities of the method have been demonstrated for large-scale hydrodynamic problems, where we compute such important indicators as the water rise level and the pressure on the dam base in the case of a dam break or an emergency water spill and also the case of a landslide runout. The use of splitting schemes for integration of equations in time makes it possible to include other physical models into this numerical method, for example, heat exchange or heat transfer. Simulation of multiphase flows with a free boundary (including possible phase transitions, i.e., in a flood of lava) is part of our future plans.

References

1. C. Ancey, Plasticity and geophysical flows: a review. *J. Non-Newtonian Fluid Mech.* (2007) **142**, 4–35.
2. N. J. Balmforth, A. S. Burbidge, R. V. Craster, J. Salzig, and A. Shen, Viscoplastic models of isothermal lava domes. *J. Fluid Mech.* (2000) **403**, 37–65.
3. M. Bercovier and M. Engelman, A finite element method for incompressible non-Newtonian flows. *J. Comp. Phys.* (1980) **36**, 313–326.
4. T. Bisantino, P. Fischer, and F. Gentile, Rheological characteristics of debris-flow material in South–Gargano watersheds. *Nat. Hazards* (2010) **54**, 209–223.
5. J. Dent and T. Lang, A biviscous modified Bingham model of snow avalanche motion. *Ann. Glaciol.* (1983) **4**, 42–46.
6. A. Chorin, Numerical solution of the Navier–Stokes equations. *Math. Comp.* (1968) **22**, 745–762.

7. S. Cochard and C. Ancey, Experimental investigation of the spreading of viscoplastic fluids on inclined planes. *J. Non-Newtonian Fluid Mech.* (2009) **158**, 73–84.

8. G. M. Crisci, S. Di Gregorio, O. Pindaro, G. Ranieri, Lava flow simulation by a discrete cellular model: first implementation. *Int. J. Model. Simul.* (1986) **6**, 137–140.

9. R. Croce, M. Griebel, and M. A. Schweitzer, A parallel level-set approach for two-phase flow problems with surface tension in three space dimension. *Preprint No. 157*, Universitat Bonn, 2004.

10. M. A. Cruchaga, D. J. Celentano, and T. E. Tezduyar, Collapse of a liquid column: numerical simulation and experimental validation. *Comp. Mech.* (2007) **39**, 453–476.

11. D. Enright, F. Losasso, and R. Fedkiw, A fast and accurate semi-Lagrangian particle level set method. *Comp. Struct.* (2005) **83**, 479–490.

12. W. H. Herschel and R. Bulkley, Measurement of consistency as applied to rubber-benzene solutions. *Proc. Amer. Assoc. Test Mater. Part II*, (1926) **26**, 621–629.

13. A. J. Hogg and G. P. Matson, Slumps of viscoplastic fluids on slopes. *J. Non-Newtonian Fluid Mech.* (2009) **158**, 101–112.

14. R. M. Iverson, The physics of debris flows. *Reviews Geophys.* (1997) **35**, 245–296.

15. F. Losasso, F. Gibou, and R. Fedkiw, Simulating water and smoke with an octree data structure. *ACM Trans. Graphics* (2004) **23**, No. 3, 457–462.

16. J. G. Marr, A. Elverh, C. Harbitz, J. Imran, and P. Harff, Numerical simulation of mud-rich subaqueous debris flows on the glacially active margins of the Svalbard–Barents Sea. *Marine Geology* (2002) **188**, 351–364.

17. J. Martin and W. Moyce, An experimental study of the collapse of liquid columns on a rigid horizontal plane. *Philos. Trans. R. Soc. Lond. Ser. A* (1952) **244**, 312–324.

18. C. Min and F. Gibou, A second order accurate level set method on non-graded adaptive Cartesian grids. *J. Comp. Phys.* (2007) **225**, 300–321.

19. K. D. Nikitin, M. A. Olshanskii, K. M. Terekhov, and Y. V. Vassilevski, Numerical simulations of free surface flows on adaptive Cartesian grids with level set function method. Preprint is available online: dodo.inm.ras.ru/research/media/notv9.pdf, 2010.

20. K. D. Nikitin, M. A. Olshanskii, K. M. Terekhov, and Y. V. Vassilevski, A numerical method for the simulation of free surface flows of viscoplastic fluid in 3D. *J. Comp. Math.* (2011) *29*, 605–622.

21. K. D. Nikitin and Y. V. Vassilevski, Free surface flow modelling on dynamically refined hexahedral meshes. *Russ. J. Numer. Anal. Math. Modelling* (2008) **23**, 469–485.

22. H. Norem, F. Irgens, and B. Schieldrop, A continuum model for calculating snow avalanche velocities. In: *Proc. Davos Symp., Avalanche Formation, Movement and Effects*, IAHS Publ, No. 162, 1987.

23. S. Osher and R. Fedkiw, *Level Set Methods and Dynamic Implicit Surfaces.* Springer-Verlag, 2002.

24. E. N. Pelinovskii, *Hydrodynamics of Tsunami Waves*. IAP RAS, Nizhn. Novgorod, 1996 (in Russian).

25. S. Popinet, An accurate adaptive solver for surface-tension-driven interfacial flows. *J. Comp. Phys.* (2009) **228**, 5838–5866.

26. H. Samet, *The Design and Analysis of Spatial Data Structures*. Addison-Wesley, New York, 1989.

27. A. S. Sarkisyan, *Simulation of Ocean Dynamics*. Gidrometeoizdat, Leningrad, 1991 (in Russian).

28. J. Strain, Semi-Lagrangian methods for level set equations. *J. Comput. Phys.* (1999) **151**, 498–533.
29. M. Sussman, P. Smereka, and S. Osher, A level set approach for computing solutions to incompressible two-phase flow. *J. Comput. Phys.* (1994) **114**, 146–159.
30. N. L. Voltsinger, *Long Waves in Shallow Water*. Gidrometeoizdat, Leningrad, 1985 (in Russian).
31. http://www.jpl.nasa.gov/srtm/